High-Performance Current Controller of Single-phased Grid-connected Inverters

Hoang. T. Hua, Minh Y Nguyen

Abstract – *This study proposes a control scheme based on an iterative learning control approach (ILC) for single-phased grid-connected inverters using an LCL filter. The control objective is to regulate the grid current to track the reference current independent of disturbances with a minimum steady-state error. The conventional feedback control methods result in poor steady-state performance in inverter applications. Hence, the hybrid control structure in which ILC is combined with a PD controller to improve the tracking accuracy and disturbance rejection is proposed. Mathematical modeling and the design procedure concerning the stability of the system have been presented. In the proposed control scheme, a low-pass filter is used to prevent learning at high frequency which may affect the system stability. The design of the control strategy is examined through simulations in MATLAB environments.*

Keywords: *Iterative Learning Control (ILC), grid-connected inverters, current controller.*

NOMENCLATURE

i_1 : Inverter side current

i_2 : Grid side current

v_C : Filter capacitor voltage

v_{inv} : Inverter output voltage

v_g : Grid voltage

v_M : The modulation signal

L_1, L_2, C: Filter parameters

P(z) : Plant in discrete domain

e(z) : Error signal in discrete domain

u(z) : Control signal in discrete domain

y(z) : System output in discrete domain

$y_{ref}(z)$: Reference signal in discrete domain

Γ(z) : Learning function in discrete domain

β : Forgetting factor

I. Introduction

Recently, with the growth in demand for energy consumption, the distributed generation systems based on renewable energy sources (DPGS-RE) emerges as the potential solution to cope with the inexhaustible and environmental problems caused by traditional power generations which depend on fossil fuels [1]. Grid-connected inverter plays an important role in the operation of DPGS. It is responsible for the high-quality power to be injected into the unity grid

The design of the current controller has been extensively studied in the literature. The Proportional-Integral (PI) controller is widely used in the control of inverters due to its simplicity [2] [3]. In [4], the PI controller has been derived in the synchronous rotating frame. The performance of PI regulator implemented in a stationary and synchronous frame is presented in [5]. However, the PI controller exhibits drawbacks in the ability to track the sinusoidal reference current as being implemented in a stationary frame. Tracking performance is improved when the PI controller is used in a rotating frame, but this control scheme introduces a large burden in the computation effort which is undesired as the control algorithm is usually implemented MCUs or DSPs. The PI controller based on the state-space approach has been discussed in [6], which improves the transient response of the system. PI state space current controller designed by the pole placement approach was proposed in [7]. Although the state space approach can provide almost full controllability of the system, the design procedure is complex and requires experience. The other strategy is Proportional-Resonant (PR) controller [8]–[10]. The PR controller gives infinite gain for the signal with selected frequencies in theory, which extensively attenuates the harmonics in the injected current. However, the robustness of the PR controller is low. The tracking performance would be intensively reduced as there exists parameter variations in the system [11].

The Model Predictive Control (MPC) design was investigated in [12]. Although the MPC approach has shown the ability to precisely track reference current, this approach is largely affected by the model mismatch. To compensate for the issue of plant modeling, the adaptive MPC was proposed in [13]. However, this method introduced a large burden on computational resources. The author [14] presented the use of a multi-level inverter to reduce harmonic distortion. This method makes the hardware design complicated as the cascade multi-level inverter topology requires multiple DC sources for each H-bridge inverter. The sliding mode control approach has also been used for controlling the inverters. This technique

suffers the chattering effect, which leads to instability and electromagnetic interference issues [15]. The authors in [16] dealt with the chattering effect by combing sliding mode control and neural networks. The chattering issue is significantly reduced, but the neural networks require complex online computation, which is undesired in practical applications.

The learning control approaches such as repetitive control [17] or iterative learning control [18], [19] have been studied for inverter applications. The learning control strategy makes use of the information from the previous operation cycle to revise the control command in the current cycle. Therefore, these approaches are suitable for the control tasks in which the outputs and disturbance are periodic signals. Since the reference current and the disturbance caused by grid voltage are periodic in nature, the ILC algorithm becomes a suitable candidate to develop the control strategy for inverter applications. ILC has an excellent ability in eliminating periodic disturbances, but it cannot compensate for the non-repeating disturbance which can randomly present in the operation of inverters and usually results in low performance in transient dynamics.

In this paper, the feedback controller with the use of an ILC algorithm is proposed for developing the control strategy for single-phased grid-connected inverters. The feedback control of the grid current is used to stabilize the closed-loop system under non-repeating disturbances and improve the control performance in the transient state. The ILC controller guarantees the low steady-state error of the waveform of the injected current which is required for high-quality power to be injected into the grid. The rest of the paper is organized as follows: Fundamental of ILC algorithm is presented in Section II. The dynamic model and the proposed control structure are analyzed in Section 3. Section 4 presents the control design of the controller parameters. The simulation results are provided in Section 5. Finally, the conclusion is given in Section VI.

II. OVERVIEW OF ITERATIVE LEARNING CONTROL

ILC is the intelligent control algorithm that could be able to provide precise control for the system in which the output of the system repeats trial-to-trial. The basic idea of ILC is to use the information of the previous operating cycle to generate the command for the system in the next cycle. The system performance is improved after every learning cycle [20], [21]. In order to exploit the ILC approach, the plant is assumed to have the following criteria [22]:

1) The length of each iteration is fixed.
2) The system returns to the same condition at the start of each iteration.
3) The measurement noise of the output is small.
4) The system is time-invariant within the repetitions.
5) The system is time-invariant within the repetitions.

Considering the discrete plant $P(z)$ which is assumed to have the above criteria. Fig. 1 illustrates the ILC control scheme to apply to the plant $P(z)$. The notation i denotes the iteration i. The reference $y_{ref}(z)$ and disturbance $d(z)$ are repetitive within the iteration domain. The block z^{-N} represents the one cycle delay block, where N is the number of samples per one cycle. The zero tracking error is archived as the output $y(z)$ is identical to the reference $y_{ref}(z)$. At that time, the error $e_i(z)$ equals to zero and the control effort only depends on the signal $u_i(z)$.

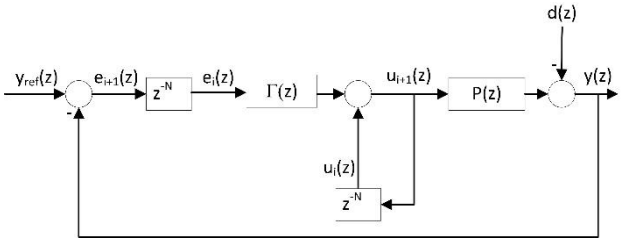

Fig. 1. Block diagram of ILC algorithm applied to plant P(z).

The control signal is determined as:

$$u_{i+1}(z) = u_i(z) + \Gamma(z)e_i(z) \quad (1)$$

Where $u_i(z)$ is the control signal at iteration i, $e_i(z)$ is the error signal at iteration i, and $\Gamma(z)$ is the learning function.

From (1) and the system dynamic in Fig. 1, the relation between the error signal of two consecutive iterations is expressed as:

$$e_{i+1}(z) = (1 - P(z)\Gamma(z))e_i(z) \quad (2)$$

The error signal is decay over subsequent iterations if the following condition fulfills:

$$\left|1 - P(z)\Gamma(z)\right|_{z = e^{j\omega T}} < 1, \forall \omega \in (0, \frac{\pi}{T}) \quad (3)$$

Where T is sampling interval, the value of $\left|1 - P(z)\Gamma(z)\right|_{z = e^{j\omega T}}$ is the decay factor. The error signal would converge to zero faster as the decay factor is smaller. The condition (3) is archived as the Nyquist plot of $P(z)\Gamma(z)$ lies on the right-half plane [23].

The error convergence characteristic can only be obtained if the system holds five assumptions as mentioned above. However, the grid-connected inverter considered in this paper may not ensure these assumptions. The initial conditions at different iteration may not the same, or the measurement noise is high in practical applications. To deal with this problem, the modified ILC scheme with the introduction of the forgetting factor is given. The scheme was verified that it can improve the robustness of the control structure [24]. The modified learning algorithm with the forgetting factor β is expressed as:

$$u_{i+1}(z) = (1- \beta)u_i(z) + \Gamma(z)e_i(z) \quad (4)$$

It is shown in [25] that the introduction of the forgetting factor would increase the robustness, but it also affects the tracking performance of the controller. Therefore, the value of the forgetting factor should be sufficiently small in order to achieve robustness, while keeping the acceptable error bound. The new relation of the error signals in two consecutive iterations becomes:

$$e_{i+1}(z) = (1 - P(z)\Gamma(z))e_i(z) + \beta P(z)u_i(z) \quad (5)$$

As the forgetting factor β is sufficiently small, the convergence condition (3) can sill be used to ensure the error convergence.

III. Current Controller for Single-Phased Grid-Connected Inverter

III.1. Dynamic model of Single-phase grid-tied inverter

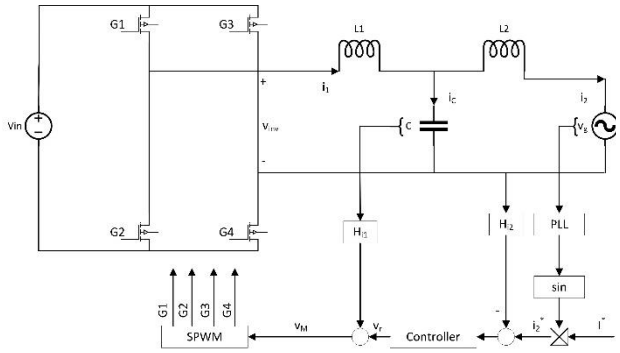

Fig. 2. Single-phase grid-connected inverter.

The typical topology of a single-phased grid-connected inverter is shown in Fig. 2. Where L_1, L_2, C are the parameters of the filter, i_1, i_2, v_C, v_{inv}, and v_g are the inverter side current, grid side current, filter capacitor voltage, inverter output voltage, and grid voltage, respectively. Unipolar sinusoidal pulse width modulation (SPWM) technique is used for the grid-connected inverter. The angle of the grid voltage θ is obtained by the phase-locked loop (PLL). The amplitude of the reference current I^* is determined by the outer power loop which calculated the desired power to be injected to the grid [26]. The reference current is then generated by $i_2^* = I^*\sin(\theta)$. The error signal is $e = i_2^* - i_2$. The error is fed to the current controller. The modulation signal is generated by adding the negative feedback of the capacitor current to the output of the current controller for damping purpose. The modulation signal is the input of the modulation module which generates the control signals for the power switches G_1, G_2, G_3, G_4.

The VSI is connected to the grid through the LCL filter. Since the switching frequency is significantly larger than the modulation signal, the dynamics of H-bridge can be ignored [27]. The inverter model mainly depends on the model of the filter. The output voltage of H-bridge inverter is defined as $v_{inv} = k_{pwm}v_M$, where v_M is the modulation signal and k_{pwm} could be determined as $k_{pwm} = \frac{V_{in}}{V_{carrier}}$. The inverter model could be written as:

$$\begin{bmatrix} \frac{di_1}{dt} \\ \frac{dv_C}{dt} \\ \frac{di_2}{dt} \end{bmatrix} = \begin{bmatrix} 0 & -\frac{1}{L_1} & 0 \\ \frac{1}{C} & 0 & -\frac{1}{C} \\ 0 & \frac{1}{L_2} & 0 \end{bmatrix} \begin{bmatrix} i_1 \\ v_C \\ i_2 \end{bmatrix} + \begin{bmatrix} \frac{k_{pwm}}{L_1} \\ 0 \\ 0 \end{bmatrix} v_M + \begin{bmatrix} 0 \\ 0 \\ \frac{-1}{L_2} \end{bmatrix} v_g$$

$$y = \begin{bmatrix} 0 & 0 & 1 \end{bmatrix} \begin{bmatrix} i_1 \\ v_C \\ i_2 \end{bmatrix} \quad (6)$$

The LCL resonant frequency is expressed as:

$$f_r = \frac{1}{2\pi}\sqrt{\frac{L_1 + L_2}{L_1 L_2 C}} \quad (7)$$

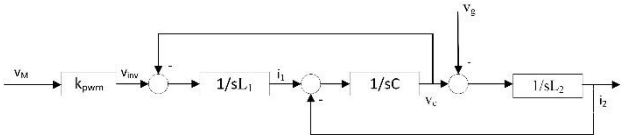

Fig. 3. Block diagram of plant inverter.

The inverter dynamic could be analyzed in the frequency domain as depicted in Fig. 3. The current injected into the grid can be derived as:

$$i_2(s) = \frac{k_{pwm}}{s^3 L_1 L_2 C + s(L_1 + L_2)} v_M(s) - \frac{(s^2 L_1 C + 1)}{s^3 L_1 L_2 C + s(L_1 + L_2)} v_g(s) \quad (8)$$

According to (9), the injected current consists of two components. The first term is affected by the control signal, while the second term is involved by the grid voltage. Our control objective is to keep the injected current the same as the waveform of the reference current signal by adjusting the modulation signal v_M. The second component is treated as disturbances. As the disturbance caused by grid voltage is a repeated signal, the control problem could be tackled by the ILC approach. The model of the LCL grid-connected inverter can be expressed as:

$$i_2(s) = P(s)v_M(s) - d(s) \quad (9)$$

Where plant $P(s) = \frac{k_{pwm}}{s^3 L_1 L_2 C + s(L_1 + L_2)}$, and disturbance $d(s) = \frac{(s^2 L_1 C + 1)}{s^3 L_1 L_2 C + s(L_1 + L_2)} v_g(s)$.

III.2. Capacitor current feedback active damping

The LCL filter possesses significant advantages over

other filter topologies in terms of the dynamic response of the system and power losses [28]. However, the stability of the LCL filter is a critical problem in designing the control system. Fig. 5 depicts the bode diagram of uncompensated plant P(s). An abrupt phase step down with the large resonance peak at the resonance frequency introduces the instability of the system [29] by introducing the closed-loop right half plane poles.

Various techniques have been proposed to damp the Various techniques have been proposed to damp the resonance peak. Passive damping methods by adding passive elements into the network have been presented in [30]. The damping method with a resistor in parallel with the filter capacitor is the most preferable choice in theory as it can effectively damp the resonance peak and has little effect on the dynamic of the filter at the frequency which is lower or higher than the resonance frequency. However, this method introduces the highest power loss because the voltage of the capacitor is approximately the grid voltage. In practice, the damping method with a resistor in series with the capacitor is the most common approach. Despite the simple implementations, the demerit of the passive damping method is that these methods introduce additional losses and increase the size and cost of the product. Active damping methods such as capacitor current feedback [31], virtual resistor [32], and band-stop filtering [33],...have been proposed to deal with the disadvantage of passive damping methods. In this paper, the capacitor current feedback proposed in [31] is used due to its simplicity and effectiveness. The block diagram of the damped system by the capacitor current feedback method is shown in Fig. 4. By moving the capacitor current feedback to the input of k_{pwm}, the system has the same dynamic as the filter with a resistor in parallel with the filter capacitor. The active damping method allows the filter to obtain the damping performance as in the case that a resistor is connected in parallel with the capacitor and does not introduce power losses. The bode diagram of the damped systems by different values of the resistor is illustrated in Fig. 5. The gain margin and phase margin are now positive, so the closed-loop system is stable.

After applying capacitor the current feedback damping, the resonance frequence is given by:

$$f_{resonance} = \frac{1}{2\pi}\sqrt{\frac{L_1 + L_2}{L_1 L_2 C}} \tag{10}$$

The design of damping coefficient has to deal with the trade-off between the damping ability and the phase margin. The larger damping cofficient can damp the resonance peak effectively but also reduce the phase margin. The value of damping resistor is chosen as in equation (11) [34].

$$R = \frac{1}{3}\frac{1}{2\pi f_{resonance} C} \tag{11}$$

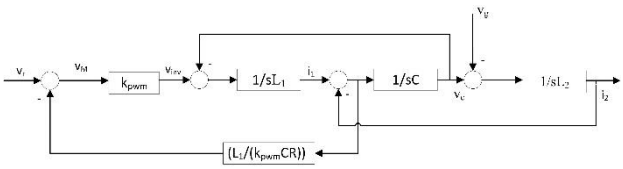

Fig. 4. Capacitor current feedback damping method.

III.3. Proposed control structure

The block diagram of the proposed control scheme is depicted in Fig. 6. Due to the behavior of the ILC approach, the control system is implemented in a digital manner. From (9), the dynamic of the system with the sampling period T is obtained by:

$$i_2(z) = P(z)v_M(z) - d(z) \tag{12}$$

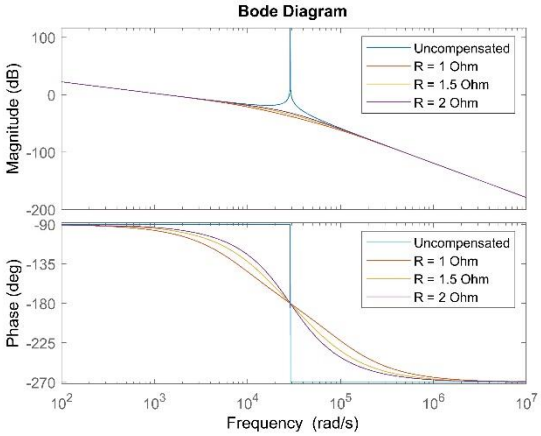

Fig. 5. Bode diagram of plant P(s).

The current controller is the combination of three components, namely the desired current feed-forward path, the feedback PD signal, and the ILC signal. The feed-forward path plays a major part in the control effort, while the ILC signal is considered the correction signal which minimizes the error at a steady state. The conventional feedback controller is added to improve the transient response of the system, but the integral part of the feedback controller is ignored due to the small steady-state error of the system.

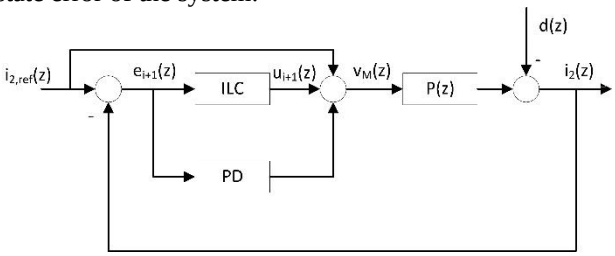

Fig. 6. Bode diagram of the proposed control scheme for single-phased grid-connected inverter.

The control signal at iteration i + 1 is calculated by:

$$v_M(z) = i_{2,ref}(z) + u_{i+1}(z) + G_{PD}(z)e_{i+1} \tag{13}$$

Where i is the iteration, $i_{2,ref}(z)$ is the desired current, $u_{i+1}(z)$ is the output of ILC algorithm at iteration i + 1, G_{PD} is the transfer function of PD controller, and e_{i+1} is the error in iteration i + 1.

The transfer function of PD controller is given as follows:

$$G_{PD} = k_p + k_d \frac{z - 1}{Tz} \quad (14)$$

The parameters k_p, k_d, T are the proportional gain, the derivative gain, and the sampling time respectively.

The P-type scheme with a forgetting factor is chosen to implement ILC algorithm. The learning function is chosen as $\Gamma(z) = z^x \alpha F(z)$ with α is the learning gain, F(z) is the filter to prevent the high frequency learning, and z^x is the advanced operator to compensate the phase lag caused by the filter. The learning algorithm is determined as:

$$u_{i+1} = (1-\beta)u_i(z) + \Gamma(z)e_i(z) \quad (15)$$

From (11) and (13). The control signal at iteration i+1 is derived as:

$$v_M(z) = i_{2,ref}(z) + (1-\beta)u_i(z) + \alpha z^x F(z)e_i + G_{PD}(z)e_{i+1} \quad (16)$$

Substitute (14) into the dynamic of the system (10). The error at iteration i+1 is obtained as:

$$e_{i+1} = \left(1 - \frac{\alpha z^x F(z)P(z)}{1 + P(z)G_{PD}(z)}\right)e_i(z) + \frac{\beta P(z)}{1 + P(z)G_{PD}(z)}u_i(z) \quad (17)$$

Now the convergence condition becomes:

$$\left|1 - \frac{\alpha z^x F(z)P(z)}{1 + P(z)G_{PD}(z)}\right|_{z = e^{j\omega T}} < 1, \forall \omega \in (0, T) \quad (18)$$

The condition (16) is identical to the condition (3) with the plant P(z) being replaced by the closed-loop transfer function $\frac{\alpha z^x F(z)P(z)}{1 + P(z)G_{PD}(z)}$. The design objective is to determine the parameters of PD-controller, the forgetting factor, and the learning function Γ(z) so that the condition (16) is satisfied. There will always exist a constant α satisfied the condition (16) if the Nyquist plot of the function $\frac{\alpha z^x F(z)P(z)}{1 + P(z)G_{PD}(z)}$ lies in the right-half plane. To achieve the fast error convergence, the value of α needs to be chosen so that the decay factor $\left|1 - \frac{\alpha z^x F(z)P(z)}{1 + P(z)G_{PD}(z)}\right|$ is minimized.

IV. Control Design

In this section, the design of the proposed control algorithm is presented. Considering the inverter system in [31] with the value of damping resistor which has the parameters as in Table I.

First, the digital model of the inverter system is calculated. As the dynamic of the system with the damping method by the capacitor current feedback is the same as the dynamic of the system using the passive damping method with a resistor in parallel with the capacitor of the LCL filter, we can use the mathematical model of the passive damping method to describe the dynamic of the system. We obtain the system dynamic as:

$$i_2(s) = P(s)v_M(s) - d(s) \quad (19)$$

TABLE I
INVERTER SPECIFICATIONS

Parameter	Symbol	Value	Parameter	Symbol	Value
Grid voltage (RMS)	V_g	220 V	Amplitude of triangular wave	$V_{carrier}$	3.05 V
Fundamental frequency	f_0	50 Hz	Switching frequency	f_s	10 kHz
Inverter side inductor	L_1	600 μH	Output power	P_o	6 kW
Filter Capacitor	C	10 μF	Injected gird current feedback coefficien	H_{12}	0.15
Grid side inductor	L_2	150 μH	Damping resistor	R	1.5 Ω
Grid side inductor	V_{DC}	360 V			

where the plant: $P(s) = \frac{k_{pwm}}{L_1L_2Cs^3 + \frac{L_1L_2Cs^2}{R} + (L_1 + L_2)s}$

, and the disturbance

$$d(s) = \frac{\left(Cs + \frac{1}{R} + 1\right)}{L_1L_2Cs^3 + \frac{L_1L_2Cs^2}{R} + (L_1 + L_2)s} v_g(s)$$

The discrete model of P(s) using zero-order-hold (ZOH) and sampling frequency of 40 kHz is obtained as:

$$P(z) = \frac{0.006271z^2 + 0.132z + 0.00164}{z^3 - 1.436z^2 + 0.5057z - 0.06948} \quad (20)$$

The parameters of PD controller are obtained by PID-Tunner application in Matlab software. The gains are determined as $k_p = 0.984105920190842$, and $k_d = 6.59449920156203 \times 10^{-5}$.

According to condition (16), the Nyquist plot closed-loop transfer function $\frac{\alpha z^x F(z)P(z)}{1 + P(z)G_{PD}(z)}$ must lie in the right-half plane. The Nyquist plot of the uncompensated closed-loop system $\frac{P(z)}{1 + P(z)G_{PD}(z)}$ is given in Fig. 7. The Nyquist plot exceeds the right-half plane on the frequency greater than 719 Hz. Therefore, the updating control signals in the frequency range higher than cut-off frequency of 719 Hz need to be filtered. The filter F(z) was designed to be an eighth-order uniform FIR filter to attenuate the learning at high frequency range. The FIR filter is defined:

$$F(z) = \frac{1}{9}\frac{z^{-8}+z^{-7}+z^{-6}+z^{-5}+z^{-4}+z^{-3}+z^{-2}+z^{-1}+1}{1} \quad (21)$$

The advanced operator is chosen as z^{10} to compensate the phase shift. The Nyquist plot of the filtered closed-loop system $\frac{z^{10}F(z)P(z)}{1+P(z)G_{PD}(z)}$ is shown in Fig. 8. The Nyquist plot almost lies on the right-half plane. Although the plot crosses the left-half plane at the frequency of 4443 Hz, the stability of the system is not affected because the attenuation of the system is significantly low, below -50 dB.

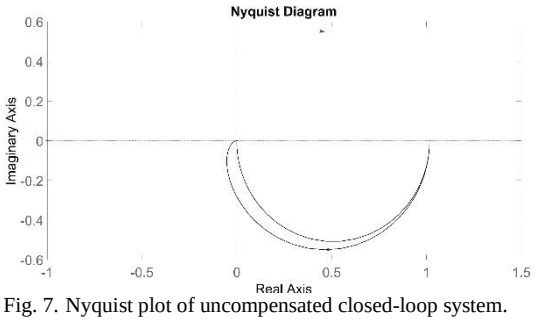

Fig. 7. Nyquist plot of uncompensated closed-loop system.

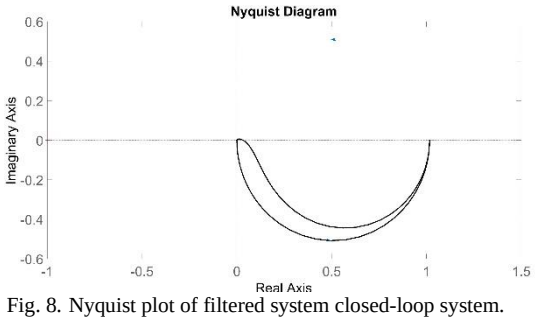

Fig. 8. Nyquist plot of filtered system closed-loop system.

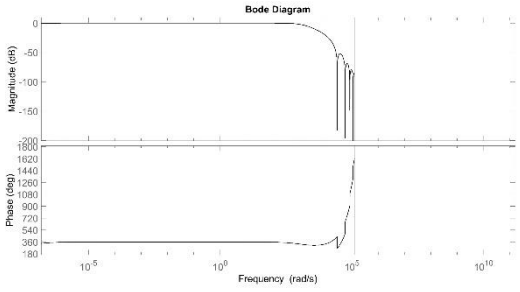

Fig. 9. Bode plot of closed-loop system with a FIR filter.

As seen in Fig. 9, the magnitude of the filtered system is almost unity on the low frequency range (below cut-off frequency). Consequently, the learning gain α is chosen as 1 to minimize the decay factor. The value of forgetting factor is selected as 0.001.

V. Simulation Results

The proposed controller has been verified by simulation using Sim Power and Simulink toolboxes in MATLAB environment.

Fig. 10(b) shows the waveforms of the reference and the grid current when the controller without the FIR filter is applied. The system becomes unstable and the error convergence cannot be archived. As the FIR filter is applied, the grid current gradually tracks the reference and the error almost converges to zero. The steady-state response at rated load,the rms value of grid current $i_{2,rms} = 27.27A$, is illustrated in Fig. 11. The total harmonic distortion (THD) is about 0.77%, and the rms value of i_2 is 27.28A. The transient response of the system is also investigated. As seen in Fig. 12, the controller requires about one cycle to derive the current to follow the new reference value.

In [31], the factor to evaluate the steady-state error is designated by the amplitude error E_A. The amplitude error is defined as:

$$E_A = \left|\frac{I_2 - I_{ref}}{I_{ref}}\right| \quad (22)$$

Where I_2, and I_{ref} are the rms value of the grid current and reference current respectively.

Fig. 13 illustrates the current waveform at rated load with different power factor (PF) references. The steady-state errors are summarized in Table II. The performance of the proposed ILC controller is compared with the results by the PI and PR controller used in [31]. The data show that the proposed controller provides better performance in tracking ability over these two feedback controllers.

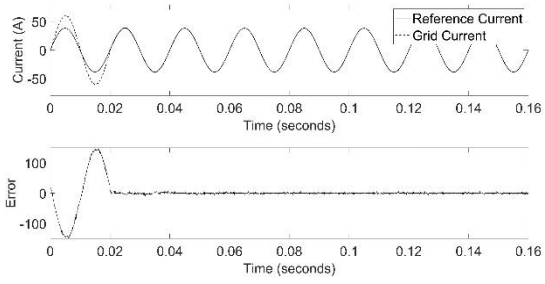

(a) System response without filter

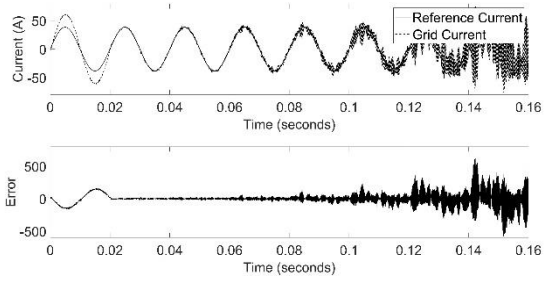

(b) System response without FIR filter

Fig. 10. System responses.

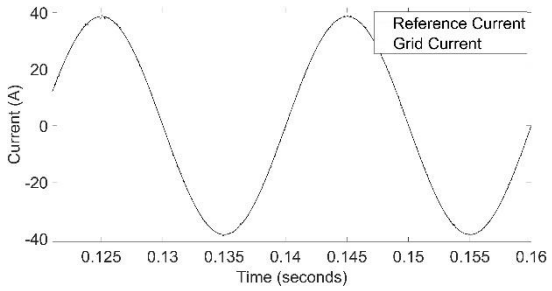

Fig. 11. Steady-state response.

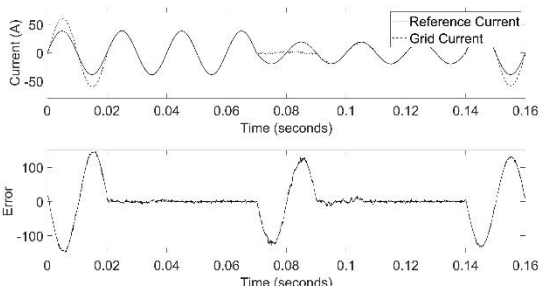

Fig. 12. Injected current jumps between rated load and half-load.

TABLE II
STEADY-STATE ERRORS AT DIFFERENT REFERENCE POWER FACTORS

Reference PF	**Measured PF**			**RMS value of grid current (A)**			**The amplitude error**		
	PI	PR	Proposed ILC	PI	PR	Proposed ILC	PI	PR	Proposed ILC
1	0.995	0.999	0.999	27.13	27.1	27.28	0.005	0.006	0.0004
0.8 capacitive	0.805	0.999	0.999	26.11	27.26	27.29	0.042	0.001	0.001
0 capacitive	0.018	-0.028	0.006	25.18	27.29	27.29	0.076	0.001	0.001
0.8 inductive	0.801	0.820	0.798	28.39	27.26	27.29	0.041	0.001	0.001
0 inductive	0.028	-0.019	0.005	28.98	27.29	27.29	0.063	0.001	0.001

Another concern in the quality of the injected current is the THD. The THD of the current to be put in the grid has to be satisfied the IEEE 929 standard, which allows the limit value of 5% for the THD factor [35]. As mentioned in (8), the grid current is combined of the component of the modulation signal and the component of the grid voltage. The LCL inverter can be used to eliminate the distortion caused by the modulation signal, but attenuating the harmonic distortion results from the harmonic contained in grid voltage is more challenging. Wang et al. have investigated the problem with the grid voltage for the same model in Table I [36].

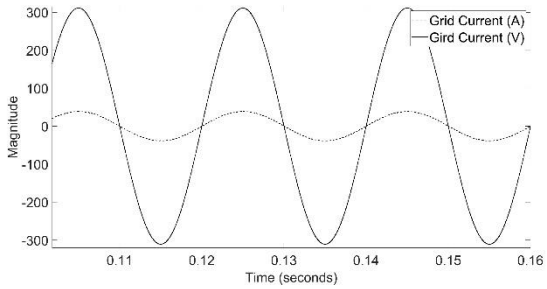

(a) PF = 1.

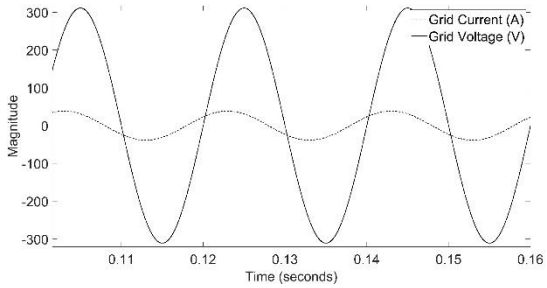

(b) PF = 0.8 Capacitive.

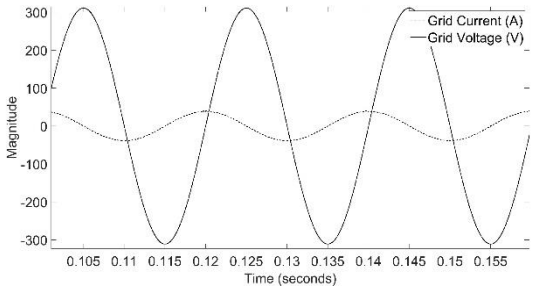

(c) PF = 0 Capacitive.

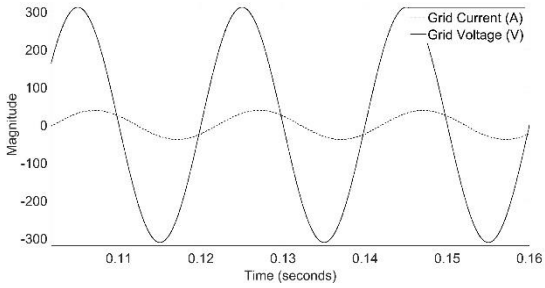

(d) PF = 0.8 Inductive.

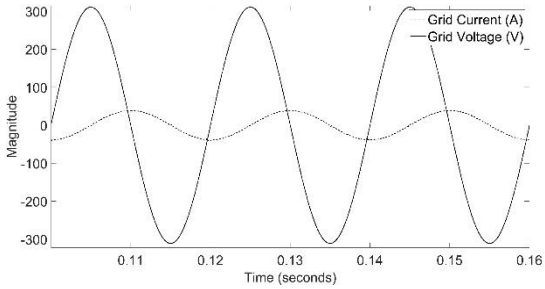

(e) PF = 0 Inductive.

Fig. 13. System response with different reference power factors.

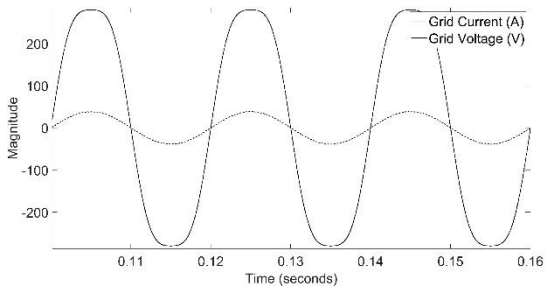

Fig. 14. Simulation result in case the grid voltage contains the 3rd harmonics.

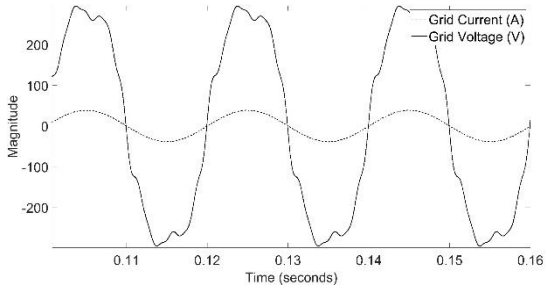

Fig. 15. Simulation result in case the grid voltage contains the 3rd, 5th, 7th, 9th, 11th, 13th harmonics.

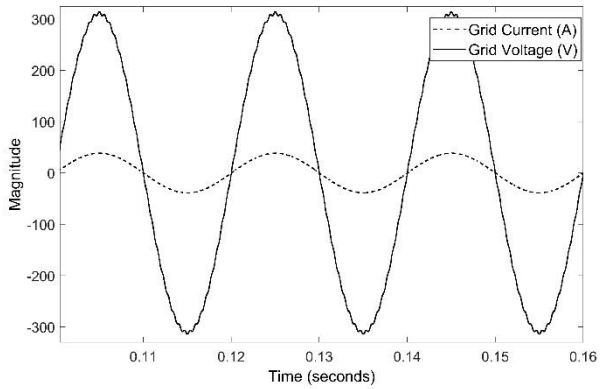

Fig. 16. Simulation result in case the grid voltage contains the 33rd harmonics.

Fig. 14 shows the simulation result when the inverter operates in rated load for the case there is the 3rd harmonic contained in the grid voltage. The magnitude of the harmonic is 10% and the phase is $0°$ with respect to the reference current. The THD of the injected current is 0.87%, while the corresponding THD in [36] is 1.27%.

Fig. 15 illustrates the simulation result when the inverter operates in rated load with the grid voltage containing 3rd, 5h, 7th, 9th, 11th, and 13th harmonics. The magnitudes with respect to the reference current are 10%, 5%, 3%, 3%, 2%, and 2%, and the corresponding phases are $0°$, $90°$, $0°$, $0°$, $0°$, and $0°$. The THD of the injected current is obtained as 0.85%, whereas the proportional feed-forward scheme and the derivative feedforward scheme in [36] result in 2.61% and 1.42% respectively.

The simulation result when the inverter operates in rated load, and the grid voltage contains the 33rd harmonic. The magnitude and the phase with respect to the reference current are 0.01% and $0°$ respectively. The THD of the injected current is 0.73% which is significantly improved with the full feedforward scheme in [36] with the THD of 1.31%.

VI. Conclusion

This study proposes a control scheme based on an iterative learning control approach for a single-phase grid-connected inverter with an LCL filter. The capacitor current feedback is exploited to tackle the resonance hazard problem of the LCL filter. As the grid current and the disturbance caused by grid voltage are periodic signals, ILC emerges as the appropriate approach for designing the current controller for the grid current. The design of the controller concerning the convergence condition is presented. The stability of the system is ensured by preventing the learning at the frequency range which makes the Nyquist plot of the system exceed the right-half plane. The ILC control scheme with the PD controller connected in parallel is proposed to improve the system response in the transient period and deal with the non-repeating disturbances. Simulations have proven the effectiveness of the control scheme and design. The control scheme in this paper has achieved a fast convergence rate in which the output tracks the reference signal within one learning iteration after the reference signal changes. However, the control design requires the mathematical model of the plant. Many plants are very complex to get models in real life. In the future, the study will be extended in the convergence rate of the systems which do not have precisely model.

VII. References

[1] S. O. Amrouche, D.Rekioua, T.Rekioua, and S.Bacha,"Overview of energy storage in renewable energy systems," *International Journal of Hydrogen Energy*, vol. 41, no. 45, pp. 20914–20927, 2016.

[2] M. Ciobotaru, R. Teodorescu, and F. Blaabjerg, "Control of single-stage single-phase pv inverter," *EPE Journal*, vol. 16, no. 3, pp. 20–26, 2006.

[3] K. Chaniago, J. Selvaraj, and N. Rahim, "Implementation of singlephase grid connected inverter using tms320f2812," in *2008 3rd IEEE Conference on Industrial Electronics and Applications*, pp. 1498–1502, IEEE, 2008.

[4] E. Twining and D. G. Holmes, "Grid current regulation of a three-phase voltage source inverter with an lcl input filter," *IEEE transactions on power electronics*, vol. 18, no. 3, pp. 888–895, 2003.

[5] D. N. Zmood, D. G. Holmes, and G. Bode, "Frequency domain analysis of three phase linear current regulators," in *Conference Record of the 1999 IEEE Industry Applications Conference. Thirty Forth IAS Annual Meeting (Cat. No. 99CH36370)*, vol. 2, pp. 818–825, IEEE, 1999.

[6] A. Draou, Y. Sato, and T. Kataoka, "A new state feedback based transient control of pwm ac to dc

voltage type converters," *IEEE transactions on power electronics*, vol. 10, no. 6, pp. 716–724, 1995.

[7] J. Dannehl, F. W. Fuchs, and P. B. Thøgersen, "Pi state space current control of grid-connected pwm converters with lcl filters," *IEEE Transactions on Power Electronics*, vol. 25, no. 9, pp. 2320–2330, 2010.

[8] R. Teodorescu, F. Blaabjerg, U. Borup, and M. Liserre, "A new control structure for grid-connected lcl pv inverters with zero steady-state error and selective harmonic compensation," in *Nineteenth Annual IEEE Applied Power Electronics Conference and Exposition, 2004. APEC'04.*, vol. 1, pp. 580–586, IEEE, 2004.

[9] X. Yuan, W. Merk, H. Stemmler, and J. Allmeling, "Stationary-frame generalized integrators for current control of active power filters with zero steady-state error for current harmonics of concern under unbalanced and distorted operating conditions," *IEEE transactions on industry applications*, vol. 38, no. 2, pp. 523–532, 2002.

[10] N. Zhang, H. Tang, and C. Yao, "A systematic method for designing a pr controller and active damping of the lcl filter for single-phase gridconnected pv inverters," *Energies*, vol. 7, no. 6, pp. 3934–3954, 2014.

[11] H. Xiao, M. Li, L. Wu, and M. Cheng, "A novel current controller for grid-connected voltage-source-inverters," *IEEE Transactions on Industrial Electronics*, 2020.

[12] Andang, A., Hartarti, R., Manuaba, I., Kumara, I., Harmonics Reduction on Electric Power Grid Using Shunt Hybrid Active Power Filter with Finite-Control-Set Model-Predictive Control, (2020) International Review on Modelling and Simulations (IREMOS), 13 (1), pp. 52-62.

[13] P. Li, Z. Song, H. Zhang and W. Jin, "Adaptive Finite Control Set Model Predictive Control Scheme for Single-phase Inverters with LCL Filter," 2020 39th Chinese Control Conference (CCC), Shenyang, China, 2020, pp. 5270-5275.

[14] Chaithanakulwat, A., Simulation of Power Transmission from Photovoltaics into a Single-Phase Grid System Using Eleven-Level Cascade Multilevel Inverter, (2020) International Review on Modelling and Simulations (IREMOS), 13 (2), pp. 91-96.

[15] Kumar, Nayan, Tapas Kumar Saha, and Jayati Dey. "Sliding-mode control of PWM dual inverter-based grid-connected PV system: Modeling and performance analysis." IEEE Journal of Emerging and Selected Topics in Power Electronics 4, no. 2 (2015): 435-444.

[16] Y. Zhu and J. Fei, "Adaptive Global Fast Terminal Sliding Mode Control of Grid-connected Photovoltaic System Using Fuzzy Neural Network Approach," in IEEE Access, vol. 5, pp. 9476-9484, 2017.

[17] S.-H. Lee, W.-J. Cha, B.-H. Kwon, and M. Kim, "Discrete-time repetitive control of flyback ccm inverter for pv power applications," *IEEE Transactions on Industrial Electronics*, vol. 63, no. 2, pp. 976–984, 2015.

[18] R. Kulawinek, K. Galkowski, L. Grzesiak, and A. Kummert, "Iterative learning control method for a single-phase inverter with sinusoidal output voltage," in *IECON 2011-37th Annual Conference of the IEEE Industrial Electronics Society*, pp. 1402–1407, IEEE, 2011.

[19] L. Ben-brahim, M. Benammar, and M. Alhamadi, "A new iterative learning control method for pwm inverter current regulation," in *The Fifth International Conference on Power Electronics and Drive Systems, 2003. PEDS 2003.*, vol. 2, pp. 1460–1465, IEEE, 2003.

[20] J.-X. Xu and Y. Tan, *Linear and nonlinear iterative learning control*, vol. 291. Springer, 2003.

[21] D. A. Bristow, M. Tharayil, and A. G. Alleyne, "A survey of iterative learning control," *IEEE control systems magazine*, vol. 26, no. 3, pp. 96–114, 2006.

[22] H.-S. Ahn, Y. Chen, and K. L. Moore, "Iterative learning control: Brief survey and categorization," *IEEE Transactions on Systems, Man, and Cybernetics, Part C (Applications and Reviews)*, vol. 37, no. 6, pp. 1099– 1121, 2007.

[23] J. Hatonen, "Issues of algebra and optimality in iterative learningcontrol," 2004.

[24] S. Arimoto, T. Naniwa, and H. Suzuki, "Robustness of p-type learningcontrol with a forgetting factor for robotic motions," in29th IEEEConference on Decision and Control, pp. 2640–2645, IEEE, 1990.

[25] D. Wang, "On d-type and p-type ilc designs and anticipatory approach,"International Journal of Control, vol. 73, no. 10, pp. 890–901, 2000.

[26] T. Orłowska-Kowalska, F. Blaabjerg, and J. Rodriguez, *Advanced and intelligent control in power electronics and drives*, vol. 531. Springer, 2014.

[27] N. Mohan, T. M. Undeland, and W. P. Robbins, *Power electronics: converters, applications, and design*. John wiley & sons, 2003.

[28] M. Liserre, A. Dell'Aquila, and F. Blaabjerg, "Stability improvements of an lcl-filter based three-phase active rectifier," in *2002 IEEE 33rd Annual IEEE Power Electronics Specialists Conference. Proceedings (Cat. No. 02CH37289)*, vol. 3, pp. 1195–1201, IEEE, 2002.

[29] G. C. Goodwin, S. F. Graebe, M. E. Salgado, *et al.*, *Control system design*. Upper Saddle River, NJ: Prentice Hall,, 2001.

[30] R. Pena-Alzola, M. Liserre, F. Blaabjerg, R. Sebastian, J. Dannehl, and ´ F. W. Fuchs, "Analysis of the passive damping losses in lcl-filter-based grid converters," *IEEE Transactions on Power Electronics*, vol. 28, no. 6, pp. 2642–2646, 2012.

[31] C. Bao, X. Ruan, X. Wang, W. Li, D. Pan, and K. Weng, "Step-by-step controller design for lcl-type grid-connected inverter with capacitor–current-feedback active-damping," *IEEE Transactions on*

Power Electronics, vol. 29, no. 3, pp. 1239–1253, 2013.

[32] C. Wessels, J. Dannehl, and F. W. Fuchs, "Active damping of lcl-filter resonance based on virtual resistor for pwm rectifiers—stability analysis with different filter parameters," in *2008 IEEE Power Electronics Specialists Conference*, pp. 3532–3538, IEEE, 2008.

[33] M. Liserre, A. Dell'Aquila, and F. Blaabjerg, "Genetic algorithm-based design of the active damping for an lcl-filter three-phase active rectifier," *IEEE Transactions on Power Electronics*, vol. 19, no.1, pp. 76–86, 2004.

[34] M. Pastor and J. Dudrik, "Design and control of LCL filter with active damping for grid-connected inverter," 2015 International Conference on Electrical Drives and Power Electronics (EDPE), Tatranska Lomnica, Slovakia, 2015, pp. 465-469.

[35] "Ieee recommended practice for utility interface of photovoltaic (pv) systems," *IEEE Std 929-2000*, pp.i–, 2000.

[36] X. Wang, X. Ruan, S. Liu, and K. T. Chi, "Full feedforward of grid voltage for grid-connected inverter with lcl filter to suppress current distortion due to grid voltage harmonics," *IEEE Transactions on Power Electronics*, vol. 25, no. 12, pp. 3119–3127, 2010.